Vibrational spectroscopy of polyatomic materials: Semiempirical calculations of anharmonic couplings and infrared and Raman linewidths in naphthalene and PETN crystals

Andrei Piryatinski,* Sergei Tretiak, and Thomas D. Sewell
Theoretical Division, Los Alamos National Laboratory, Los Alamos, New Mexico 87545, USA

Shawn D. McGrane
Dynamic and Energetic Materials Division, Los Alamos National Laboratory, Los Alamos, New Mexico 87545, USA
(Received 25 January 2007; published 21 June 2007)

We have developed a computational approach that yields anharmonic vibrational couplings in molecular crystals. The approach is based on anharmonic vibrational potential-energy surface reconstruction starting from a normal-mode vibrational basis. The method was implemented for semiempirical Hamiltonians with periodic boundary conditions, with applications to crystalline naphthalene and pentaerythritol tetranitrate. For each material, we predicted infrared and Raman linewidths, and vibrational anharmonic couplings associated with up- and down-conversions, as well as pure-dephasing processes. Comparison is made to experimental data for Raman linewidths and averaged anharmonic couplings; reasonable agreement is obtained, suggesting that implementation of the method within a first-principles electronic structure framework is warranted.

DOI: 10.1103/PhysRevB.75.214306 PACS number(s): 63.20.Ry, 78.30.−j, 78.20.Bh, 78.30.Jw

I. INTRODUCTION

Optical spectroscopies are among the primary tools for investigating the dynamics of vibrational energy transfer and chemical reactions.[1] Techniques such as infrared (IR) absorption, temperature-dependent Raman spectroscopy, and IR pump and anti-Stokes probe can be used to probe directly the vibrational cooling processes in neat liquids, solvated molecules, and solids.[2–7] These processes are mediated by anharmonic couplings among the vibrational modes. Average anharmonic couplings can be obtained from an analysis of line broadening and gas-to-crystal-phase line shifts. Temperature variation controls the population of low-frequency modes and as a result, in a temperature-dependent experiment, one can determine which among those modes participate in the energy transfer by observing the time evolution of the associated spectral features.

Relaxation and transfer of vibrational energy in molecular crystals are determined by anharmonic couplings between the high-energy intramolecular vibrational modes and low-frequency phonons. Two physically related, albeit opposite in effect, processes can occur. First is relaxation (down-conversion) of the energy initially deposited into the higher-frequency vibrational modes, for example, using IR excitation due to electronic transitions; the second is up-pumping of the phonon energy into the high-energy modes, as in the case of shock wave loading.[3,8–11] Both processes have significant effects on the chemical reaction dynamics. The up-pumping process is widely thought to be one of the initial events in the initiation of shock-induced detonation.[3,8–11]

The spectroscopies mentioned above cannot provide selective information about the couplings among specific modes but rather provide only averaged information. This limits our insight into the energy flow pathways whose complete determination requires knowledge of all anharmonic couplings among all normal modes in the system.[12] These can, in principle, be obtained from computer simulations; the results of which can be compared to experimental observables after appropriate averaging. Good agreement between experiment and theory provides indirect validation of the theoretical method, which can then be used to draw conclusions about the underlying dynamics. Also, once validated, the theory can predict the time-dependent energy transfer for any given initial condition, which will not be possible experimentally.

Previous simulations of delocalized intermolecular modes (phonons) and localized intramolecular vibrational modes (vibrons) in molecular crystals have been performed using various degrees of approximation for the inter- and intramolecular force fields. The approaches used in the earliest studies treated only phonons within a rigid-molecule framework, and were based on empirical form intermolecular potentials with parameters fitted to experiment, or assumed an averaged anharmonic coupling between the phonons and vibrons whose value was also fitted to experiment.[2,13–15] More advanced techniques have been developed, for example, replacement of the empirical form potential with "first-principles" methods such as density-functional theory (DFT).[16–18] While these methods allow more-or-less routine electronic structure-based predictions of the vibrational normal modes, they have not been used to predict anharmonic couplings in condensed-phase materials. Our ultimate goal is to develop a computational methodology for determining the anharmonic couplings in polyatomic materials with periodic boundary conditions using recent advances in electronic structure calculations. Such an approach would eliminate the need for specification and parametrization of empirical force fields and, once validated, would be applicable to a wide variety of materials.

In this paper, we use a semiclassical approach based on an anharmonic expansion of the potential energy in terms of the vibrational normal modes of a molecular crystal. For development purposes, we employ simple semiempirical electronic structure models[19–21] (AM1 and PM3) to obtain the crystal normal modes and the cubic and quartic coupling constants among them. The approach provides phonon-

phonon, phonon-vibron, and vibron-vibron couplings. We apply the method to study the anharmonic couplings in crystalline naphthalene and pentaerythritol tetranitrate (PETN, an important energetic material), both of which are well studied experimentally. Comparison to experiment is made by calculating IR and Raman linewidths and averaged values for the phonon-phonon, phonon-vibron, and vibron-vibron couplings among selected modes. The method is described in Sec. II, results and discussion are presented in Sec. III, and concluding remarks are given in Sec. IV.

II. DESCRIPTION OF THE COMPUTATIONAL METHOD

In this section, we present a computational approach used to determine the cubic and quartic anharmonic couplings among the normal modes in a periodic molecular structure. We also provide expressions for calculating spectroscopic observables such as IR and Raman linewidth and effective anharmonic couplings that can be obtained from linear optical spectroscopies.

As input to the calculations, we use published unit-cell atomic coordinates for naphthalene and PETN obtained from x-ray scattering experiments. Using the MOPAC 2000 computational package,[22] which implements the semiempirical electronic structure models with periodic boundary conditions, we optimize the unit-cell geometries and perform a normal-mode analysis. The normal-mode eigenenergies and eigenvectors calculated by MOPAC 2000 are limited to the $\mathbf{\Gamma}$ point ($\mathbf{k}=0$) of the Brillouin zone only. Thus, in calculating experimental observables, we are not able to account for the acoustic phonons and will only account for the optical-phonon dispersion (dependence on $\mathbf{k}$) phenomenologically. Identification of the normal modes is made by comparison of computed and measured IR and Raman spectra. Mode identification was further facilitated by direct visualization of the modal atomic motions using the MOLDEN visualization package.[23]

In order to evaluate sets of the effective cubic ($B^{(3)}_{ijk}$) and quartic ($B^{(4)}_{ijkl}$) anharmonic couplings derived in the Appendix, we implemented, at the level of parallel shell script calls to MOPAC 2000 and additional homemade codes, the following computational protocol. We begin with a general expansion of the unit-cell anharmonic potential energy in mass-weighted normal modes (ξ_i)

$$V_{anh}(\xi) = \sum_{i,j,k=1}^{M} B^{(3)}_{ijk}\xi_i\xi_j\xi_k + \sum_{i,j,k,l=1}^{M} B^{(4)}_{ijkl}\xi_i\xi_j\xi_k\xi_l, \qquad (1)$$

where $M=3N-3$ is the total number of the normal modes associated with the unit cell, and N is the number of atoms in a unit cell. The Taylor expansion in Eq. (1) assumes weak anharmonic corrections induced by small nuclei displacements from the equilibrium positions. Such displacements can be initiated by an optical excitation or a small mechanical compression. The expansion has been truncated at the fourth-order terms, which represent the lowest-order contributions to processes of intermode energy transfer (cubic anharmoncity) and pure dephasing (quartic term).

First, we select a normal mode $i=n$ whose couplings with the pairs of the others ($j,k=1,2,\ldots,M$) are to be studied. Then, taking into account the index permutation symmetries of the coupling coefficients in Eq. (1), we sample the $M(M+1)/2$ possible combinations of mode n with the others. For each combination, the atomic coordinates are displaced from the equilibrium (optimized geometry) positions along the mass-weighted normal-mode eigenvectors. Each displacement is made N_d times each in the positive and negative directions. As a result, we generate $(2N_d+1)^3$ reference points for vibrational potential-energy surface reconstruction. Since the potential-energy surface curvature (eigenenergy) can differ significantly from one mode to the next, we control the amplitudes of the displacement steps $\Delta\xi_i$ by expressing them in units of the harmonic vibrational quanta (N_q) as $\Delta\xi_i=\sqrt{\hbar\omega_i(2N_q+1)}$. Converged single-point energies are calculated for each of the $(2N_d+1)^3$ reference points, and the resulting energy grid is fitted to Eq. (1), which requires that $N_d \geqslant 2$ due to the degree of the fitting polynomial. This procedure yields values of $B^{(3)}_{njk}$ and $B^{(4)}_{nnjk}$. Note that the quartic anharmonic constant which we calculate this way depends on only *three* independent indices. Below, we show that this is sufficient to calculate the observable linewidths.

The linewidth calculations were performed using many-body perturbation theory.[13,14,24–26] According to this theory, the total linewidth is a sum of three components

$$\Gamma^{th}(\omega_n) = \Gamma^{d}(\omega_n) + \Gamma^{u}(\omega_n) + \Gamma^{*}(\omega_n). \qquad (2)$$

The approximations involved in the derivation of the explicit expressions for these components are given in the Appendix. The first term is due to vibrational down-conversion, where the lowest-order process involves annihilation of one higher-energy ($\hbar\omega_n$) vibrational quantum and creation of two quanta with the lower energies ($\hbar\omega_j+\hbar\omega_k=\hbar\omega_n$). The detailed linewidth expression for this process depends on the cubic anharmonic couplings

$$\Gamma^{d}(\omega_n) = 18\hbar^{-1}\sum_{jk} |B^{(3)}_{njk}|^2 \rho^{d}_{jk}(\omega_n). \qquad (3)$$

The second term in Eq. (2) results from vibrational up-conversion, and the lowest-order contribution corresponds to annihilation of two vibrational quanta ($\hbar\omega_n$ and $\hbar\omega_j$) and creation of one higher-energy quantum ($\hbar\omega_k=\hbar\omega_n+\hbar\omega_j$). As above, this component of the linewidth also depends on the cubic anharmonicity

$$\Gamma^{u}(\omega_n) = 36\hbar^{-1}\sum_{jk} |B^{(3)}_{njk}|^2 \rho^{u}_{jk}(\omega_n). \qquad (4)$$

In contrast to the processes considered above, the last component in Eq. (2), pure dephasing, arises from elastic vibrational scattering, and the corresponding expression depends on the quartic anharmonic couplings among three modes

$$\Gamma^{*}(\omega_n) = 288\hbar^{-2}\sum_{jk} |B^{(4)}_{nnjk}|^2 \rho^{*}_{jk}. \qquad (5)$$

The thermally weighted joint vibrational densities of states (TJ-DOS) entering Eqs. (3)–(5) are

$$\rho^{d}_{jk}(\omega) = \frac{1}{\pi}\frac{(\bar{n}_j+\bar{n}_k+1)(\epsilon_j+\epsilon_k)}{(\omega-\omega_j-\omega_k)^2+(\epsilon_j+\epsilon_k)^2}, \qquad (6)$$

$$\rho_{jk}^{u}(\omega) = \frac{1}{\pi}\frac{(\bar{n}_j - \bar{n}_k)(\epsilon_j + \epsilon_k)}{(\omega + \omega_j - \omega_k)^2 + (\epsilon_j + \epsilon_k)^2}, \tag{7}$$

$$\rho_{jk}^{*} = \frac{1}{\pi}\frac{\bar{n}_j(\bar{n}_k + 1)(\epsilon_j + \epsilon_k)}{(\omega_j - \omega_k)^2 + (\epsilon_j + \epsilon_k)^2}. \tag{8}$$

Here and below, $\bar{n}_k = [\exp(\hbar\omega_k/k_BT) + 1]$ is the vibrational level occupation number, where k_B is the Boltzmann constant and T is the temperature.

The TJ-DOS functions project out limited subsets of the vibrational states which are coupled through the anharmonicities that contribute to the linewidths. Experimental measurements of linewidth, for example, in a temperature-dependent Raman experiment, carry only information about the anharmonic couplings between the relevant subsets of states. To compare the calculations with experiment, it is convenient to introduce the following effective down-conversion, up-conversion, and pure-dephasing anharmonic constants, respectively:

$$\langle B_d^2(\omega_n)\rangle = \frac{\sum_{jk} |B_{njk}^{(3)}|^2 \rho_{jk}^{d}(\omega_n)}{\sum_{jk} \rho_{jk}^{d}(\omega_n)}, \tag{9}$$

$$\langle B_u^2(\omega_n)\rangle = \frac{\sum_{jk} |B_{njk}^{(3)}|^2 \rho_{jk}^{u}(\omega_n)}{\sum_{jk} \rho_{jk}^{u}(\omega_n)}, \tag{10}$$

$$\langle B_p^2(\omega_n)\rangle = \frac{\sum_{jk} |B_{nnjk}^{(4)}|^2 \rho_{jk}^{*}}{\sum_{jk} \rho_{jk}^{*}}. \tag{11}$$

The normal-mode and the anharmonic coupling calculations are performed in the coordinate space of a single unit cell where the self-consistent approximation for the local fields is due to the periodic boundary conditions. This limits our ability to calculate the TJ-DOS explicitly as well as to account for the optical-phonon and -vibron dispersions. The vibrons are highly localized, and their densities of states are narrowly distributed around the central frequencies.[13] Therefore, for the vibrons, the dispersion effects can be safely neglected. In contrast, the optical-phonon modes are delocalized and have much broader energy dispersion. In the present work, we account for the energy dispersion in the TJ-DOS by choosing an adequately large value of ϵ in Eqs. (6)–(8).

III. RESULTS AND DISCUSSION

An x-ray determination of the naphthalene crystal structure[27] was used as input to MOPAC 2000. The arrangement of the two molecules in the monoclinic unit cell is depicted in Fig. 1. All the calculations for the naphthalene unit cell were performed using the AM1 semiempirical model with periodic boundary conditions. Lattice vectors for naphthalene were fixed at experimental values, since an attempt at an unconstrained optimization of the crystal failed to converge.

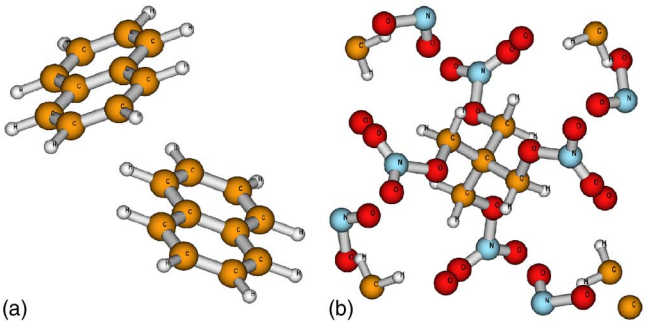

FIG. 1. (Color online) Unit-cell geometry of (a) naphthalene and (b) PETN used in the simulations. Atomic groups present in the corners of the PETN unit cell are fragments of the molecule centered at the unit-cell corners.

The PETN unit-cell geometry shown in Fig. 1(b) was taken from an x-ray determination.[28] The unit cell in this case contains two molecules and forms a body-centered-tetragonal structure. In our calculations on the PETN unit cell, we used the PM3 semiempirical model[20,21] instead of the AM1 model[19] adopted for naphthalene. The former model is calibrated to better reproduce heat of formation of energetic materials.[29,30] Periodic crystal optimizations for both constrained and unconstrained lattice lengths were performed with fixed lattice angles of 90° in each case. The differences between the normal modes for the two optimized structures thus obtained were insignificant. All subsequent calculations were performed using the experimental unit-cell parameters.

The naphthalene unit cell (36 atoms) has 105 nonzero normal-mode eigenenergies and eigenvectors. Among them, the 9 lowest-frequency modes are optical phonons, while the remaining 96 are vibrons. The constrained unit-cell optimization led to a small but negative value of the lowest normal-mode energy; this mode was ignored. The calculated IR-absorption spectrum is shown in Fig. 2(a). Its comparison with the experimentally measured Raman spectrum[7] assisted us with the normal-mode identification. We selected three normal modes, $n=8$, 14, and 81 for further analysis; among them, mode 8 is a delocalized libration (optical phonon), and modes 14 and 81 are localized skeletal vibrations (vibrons). The mode positions are marked with arrows in Fig. 2(a), and their eigenenergies (ω_n^{th}) are given in Table I(A). Based on Fig. 2(a), these modes have weak IR oscillator strength; they are, however, well resolved in the Raman spectrum,[7] and the measured frequencies at $T=298$ K (ω_n^{ex}) included in Table I compare reasonably well with the calculated ones.

The PETN unit cell (58 atoms) has 171 nonzero normal modes. As with naphthalene, the first nine modes are associated with the optical phonons, and the rest with vibrons. The calculated IR-absorption spectrum is shown in Fig. 2(b). We have compared the calculated spectrum to experimental IR and Raman results[7,18] and identified their main features. It is clear (and expected based on prior studies) that the semiempirical PM3 model significantly overestimates NO_2 stretching mode energies.[22] Measured symmetric and anti-

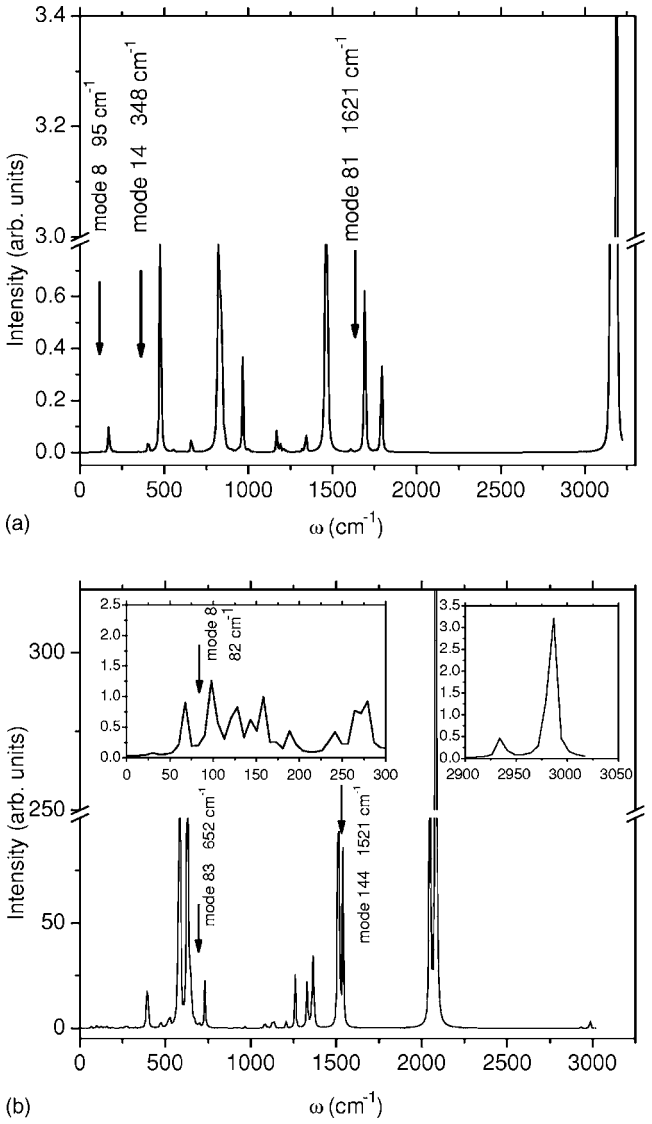

FIG. 2. Calculated IR-absorption spectra of (a) naphthalene and (b) PETN. The inset shows low- and high-frequency features of the PETN spectrum. All spectral lines have Lorentzian line shape with the central frequencies set to the normal-mode eigenenergies (no scaling applied) and the average widths to 3.0 cm^{-1}. Arrows mark the modes selected for the anharmonic coupling and linewidth calculations.

symmetric NO_2 stretches are found at around 1300 and 1650 cm^{-1}, respectively. By contrast, these modes appear in Fig. 2(b) as two intense IR features around 1500 and 2000 cm^{-1}, respectively. Although DFT calculations of gas-phase PETN at the B3LYP/6-31G^* level have been shown to compare favorably to experiment,[18] the large number of three-dimensional periodic calculations required was regarded as too large to warrant using such an expensive model chemistry in the present work, which is directed toward the development of a general methodology. Thus, we note the discrepancy and continue with the semiempirical model, which we think is sufficient for the purposes of method development which form the main emphasis in the present study. For PETN, we selected three normal modes $n=8$, 83, and 144 [Table I(B)]. The first of these is a collective unit-cell motion whose experimental counterpart was hard to identify. Mode 83 is an ONO_2 umbrella motion and mode 144 is a NO_2 symmetric stretch. Comparison to experiment in Table I indicates that the value of the ONO_2 umbrella mode is underestimated by about 100 cm^{-1}. According to Fig. 2(b), phonon mode 8 has weak IR oscillator strength, while the considered ONO_2 umbrella and NO_2 stretching modes are both IR active.

The main focus of this study is the determination of the cubic and quartic anharmonic couplings based on an anharmonic expansion of the crystal potential energy in a normal-mode basis [Eq. (1)]. For reconstruction of the potential-energy surfaces, displacements along each coupled normal mode were set to be equivalent to $N_q=5$ vibrational quanta. The number of displacements was $N_d=2$, providing a grid of 125 values of the potential energy to be fitted to Eq. (1). The IR and Raman linewidth calculations were performed according to Eqs. (3)–(5), where the TJ-DOS expressions were approximated by Eqs. (6)–(8). In this expression, the width was set to $\epsilon=50$ cm^{-1} if low-energy modes (phonons, <200 cm^{-1}) are present in the argument and $\epsilon=5$ cm^{-1} for the vibrons (>200 cm^{-1}). This parametrization was chosen to simulate qualitatively the broad density of states of the phonon mode energies and narrow density of states of the vibrons.

Figure 3 shows the results of the linewidth calculations. The total linewidth values $[2\Gamma^{th}(\omega_n)]$ agree with experiment to within an order of magnitude, and the general trends for the temperature dependence are also reproduced. The contri-

TABLE I. Comparison between calculated (*th*) and measured (*ex*) normal-mode eigenenergies (ω_n) and effective anharmonic couplings B_d and B_u in units of cm^{-1}. See text for definitions.

n	ω_n^{th}	ω_n^{ex}	B_d^{th}	B_d^{ex}	B_u^{th}	B_u^{ex}
			(A) Naphthalene			
8	96	90	0.22	0.27	0.28	0.67
14	348	389	0.13	0.25	0.23	0.20
81	1621	1630	0.08	0.82	0.15	0.12
			(B) PETN			
8	82		0.15		0.32	
83	652	755	0.16	0.14	0.19	1.09
144	1521	1292	0.09	0.6	0.28	0.39

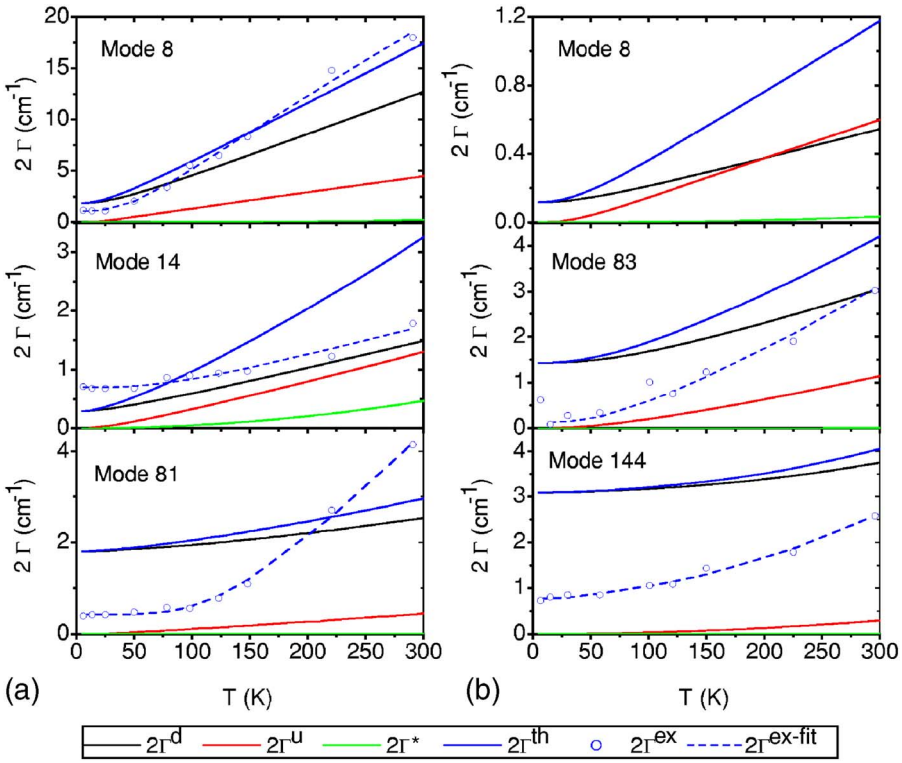

FIG. 3. (Color online) Temperature-dependent linewidth of selected (a) naphthalene and (b) PETN unit-cell modes. Shown are the calculated total linewidth (solid blue line) and its components due to phonon and/or vibron down-conversion (black line), up-conversion (red line), and pure-dephasing (green line) effects. For comparison, the experimental values (Ref. 7) are plotted (blue circles) and fitted (dashed blue line) to determine the effective anharmonic couplings B_d^{ex} and B_u^{ex} listed in Table I along with B_d^{th} and B_u^{th} [which were obtained by fitting the theoretical linewidths (solid blue line)].

butions of the linewidth components [Eqs. (2)–(5)] associated with phonon down-conversion $[\Gamma^d(\omega_n)]$, up-conversion $[\Gamma^u(\omega_n)]$, and pure dephasing $[\Gamma^*(\omega_n)]$ are also shown in the plot. At low temperatures, the down-conversion processes (black line) are the only ones present. Increasing temperature leads to increased contributions from up-conversion processes (red lines). For example, for mode 14 of naphthalene at room temperature, up-conversion and down-conversion contributions to the linewidth become comparable. The effect of pure dephasing (green lines) only becomes significant for mode 14 of naphthalene and, even then, only for temperatures higher than 100 K.

Given that the dephasing contribution is negligible, the calculated (measured) temperature-dependent linewidth curves can be fitted by a sum of modified Eqs. (3) and (4). Specifically, in these expressions, the sum over the mode indices should be dropped, and $B_{njk}^{(3)}$ replaced with B_d^{th} (B_d^{ex}) in Eq. (3) and with B_u^{th} B_u^{ex} in Eq. (4). This fit provides highly averaged "effective" up- and down-conversion anharmonic couplings directly available from the temperature-dependent Raman experiment.[7] The resulting values for the effective anharmonicities thus obtained from the curves in Fig. 3 are listed in Table I. [Usually, the prefactor 18 (36) appearing in Eq. (3) [Eq. (4)] is included into B_d^{ex} (B_u^{ex}). Here, to make an adequate comparison with the theory, we keep these prefactors in the expressions.]

A general trend which is expected for the averaged theoretically calculated anharmonicities is that their values decrease with the increasing mode energy. This reflects a notion that the phonons and low-frequency vibrons are "softer" and more anharmonic compared to the higher-frequency vibrons. This trend is clearly observed in Table I for the up-conversion anharmonicities of naphthalene. For PETN, estimated value of B_u^{th} for the phonon mode is slightly higher than corresponding values for the vibrons. The trend is also observed for B_u^{ex} and B_d^{ex} measured in PETN. Overall, averaged theoretical and experimental effective couplings are in better than order-of-magnitude agreement for nearly all modes considered, with the exceptions of the down-conversion anharmonicity of mode 81 in naphthalene and mode 144 in PETN. By looking at the experimental anharmonicity values of the latter modes, we notice that their values rise (not decrease) as the mode energies increase. In this case, a possible source of the discrepancy is the adopted approximation for the TJ-DOS. We attribute the same cause to the result for PETN mode 83, whose experimental up-conversion anharmonicity is approximately a factor of 6 larger that its calculated value.

To minimize the contribution of the line overlap causing an error in the linewidth measurements, an average of the up-conversion anharmonicities for a set of experimentally well-resolved modes was reported;[7] we compare the values in that reference to an average over the theoretical ones in Table I. The theoretical and/or experimental comparison for naphthalene is $\bar{B}_d^{th}=0.14$ cm^{-1} and $\bar{B}_d^{ex}=0.09$ cm^{-1} and for PETN, $\bar{B}_d^{th}=0.13$ cm^{-1} and $\bar{B}_d^{ex}=0.23$ cm^{-1}. This leads to the

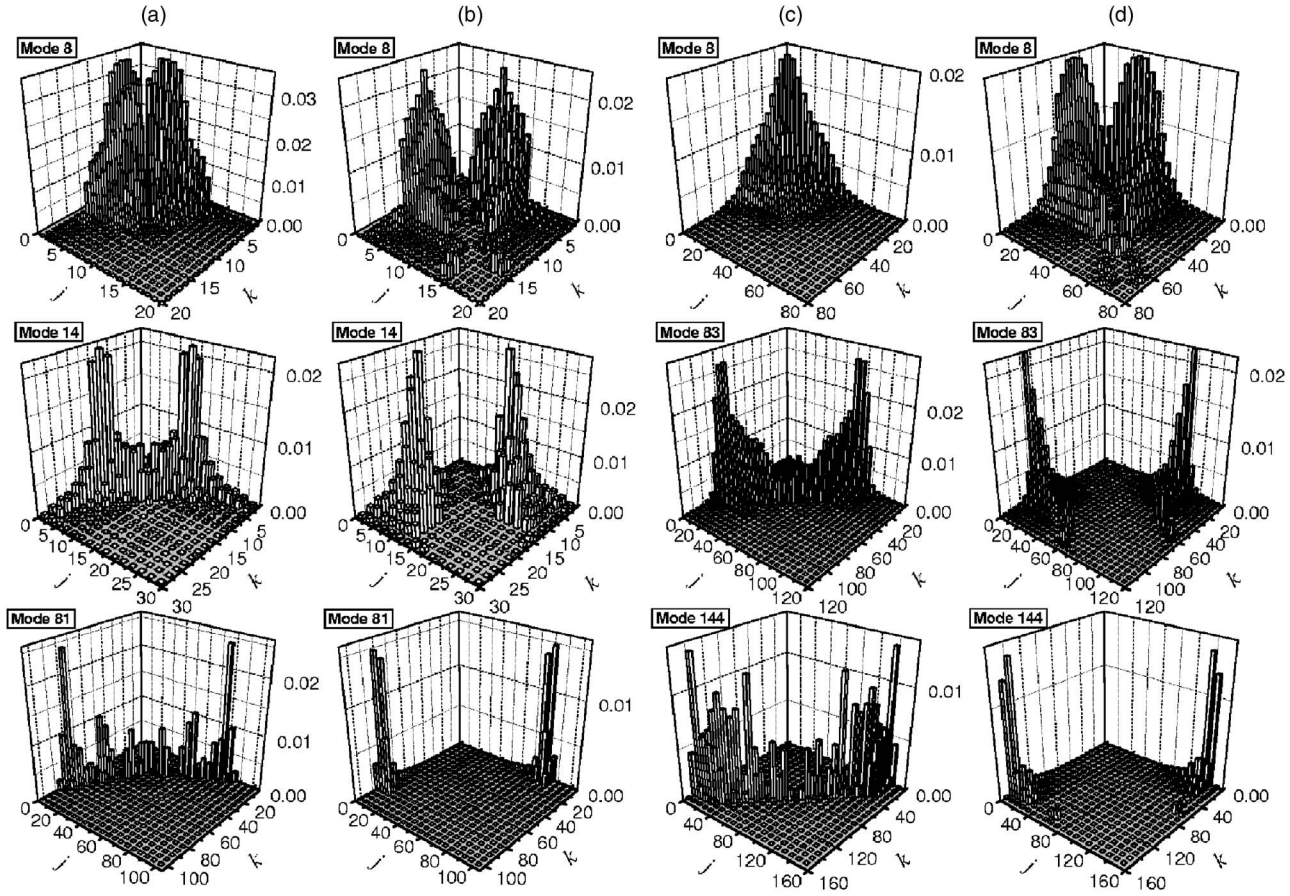

FIG. 4. Thermally weighted joint densities of states for modes j and k (TJ-DOS), determining the [(a) and (c)] energy down-conversion process [Eq. (6)] $\omega_n \rightarrow \omega_i + \omega_j$ and the [(b) and (d)] energy up-conversion processes [Eq. (7)] $\omega_n + \omega_j \rightarrow \omega_k$ and $\omega_n + \omega_k \rightarrow \omega_j$ induced by the cubic anharmonic couplings $B^{(3)}_{njk}$; calculated at a temperature of 300 K for [(a) and (b)] naphthalene and [(c) and (d)] PETN.

same conclusion as the comparison of the temperature dependent behavior, namely, that the theoretical and/or computational protocol is sufficient to reproduce the dominant qualitative features of the anharmonic couplings, and suggests that it can be used meaningfully to study the dynamics of energy transport in complicated molecular crystals.

Our ability to calculate the anharmonic couplings allows us to estimate averaged strengths of phonon-phonon, phonon-vibron, and vibron-vibron interactions in naphthalene and PETN. For energetic materials, these quantities carry information on the vibrational energy transport to and/or from the reaction centers. However, before turning our attention to the calculated numbers, we once again note that, according to Eqs. (3)–(5), the TJ-DOS factors [Eqs. (6)–(8)] select a limited subset of the vibrational states that will be coupled through anharmonic interactions. To evaluate which states participate in these processes and, therefore, which anharmonicity couplings have to be determined, we present in Figs. 4(a) and 4(b) plots of down-conversion $[\rho^d_{jk}(\omega_n)]$ given by Eq. (6) and up-conversion $[\rho^u_{jk}(\omega_n)]$ given by Eq. (7), respectively, for naphthalene at $T=300$ K as a function of the normal-mode numbers (j,k). The same quantities for PETN are presented in Figs. 4(c) and 4(d).

According to Fig. 4(a), the room-temperature linewidth of mode 8 in naphthalene is due entirely to anharmonic couplings within the manifold of phonon states $(1 \leqslant j,k < 10)$. Accordingly, averaged down-conversion anharmonic coupling of mode 8 should provide information restricted to phonon-phonon interactions. By contrast, the up-conversion TJ-DOS of the same mode involves a small amount of low-frequency vibrons $(j,k \sim 15,20)$, and the phonon-vibron contribution to the corresponding averaged anharmonicity should be higher. The vibron modes participating in the down-conversion processes can be seen to interact with states such that $\omega_n \approx \omega_i + \omega_j$, thereby forming a set of "diagonal" peaks in Figs. 4(a) and 4(c). The widths of the diagonal in Fig. 4 are determined by the adopted values for ϵ in Eqs. (6)–(8), that is, by the phonon and vibron densities of states. The up-conversion processes, $\omega_n \approx \omega_j - \omega_k$ or $\omega_n \approx \omega_k - \omega_j$, in naphthalene and PETN involve phonons and low-energy vibrons $(j,k \sim 20,40)$ as Figs. 4(b) and 4(d) show. Equations (9)–(11) used to calculate the average anharmonic couplings naturally account for the TJ-DOS limitations. By further partitioning the summations in the numerators of these equations over (j,k) indices into the sums over the phonon-phonon, phonon-vibron, and vibron-vibron mode numbers, we extract the values of each component of the interaction.

Table II summarizes the calculated values of down-conversion $(\langle B^2_d \rangle^{1/2})$, up-conversion $(\langle B^2_u \rangle^{1/2})$, and pure-dephasing $(\langle B^2_p \rangle^{1/2})$ anharmonic constants at $T=300$ K. For

TABLE II. Averaged down-conversion ($\langle B_d^2\rangle^{1/2}$), up-conversion ($\langle B_u^2\rangle^{1/2}$), and pure-dephasing ($\langle B_p^2\rangle^{1/2}$) anharmonicities calculated at $T=300$ K. Their components (see text for definitions) due to the phonon-phonon (p-p), phonon-vibron (p-v), and vibron-vibron (v-v) interactions are also listed. The quantities are given in cm^{-1} units.

	$\langle B_d^2\rangle^{1/2}$				$\langle B_u^2\rangle^{1/2}$				$\langle B_p^2\rangle^{1/2}$			
Mode n	p-p	p-v	v-v	Total	p-p	p-v	v-v	Total	p-p	p-v	v-v	Total
						(A) Naphthalene						
8	0.46	0.03		0.49	0.25	0.10		0.35	0.010	0.001		0.011
14		0.09	0.05	0.14		0.07	0.05	0.12		0.015	0.0	0.015
81		0.01	0.04	0.05		0.02	0.02	0.04		0.003	0.0	0.003
						(B) PETN						
8	0.01	0.04		0.05	0.004	0.046		0.05	0.0	0.0		
83		0.00	0.06	0.06		0.01	0.05	0.06		0.0	0.0	0.0
144		0.00	0.06	0.06		0.01	0.05	0.06		0.0	0.0	0.0

naphthalene, our calculations show that, on average, the phonon-phonon interaction (mode 8) is stronger than the other components. The vibrons (modes 14 and 81) interact with phonons and with other vibrons with comparable strengths. In contrast, for PETN, the calculated anharmonic couplings of the higher-energy modes (83, 144) are mainly due to vibron-vibron interactions. As expected, the pure-dephasing effects are negligibly weak. It is noteworthy that the total averaged anharmonic couplings in Table II and the same effective anharmonicities obtained by fitting the calculated linewidth in Fig. 3 are consistent with one another for naphthalene. For PETN, the fitting provides higher values than the TJ-DOS weighted averaging, demonstrating that the former procedure provides a crude estimate of the anharmonic couplings.

In the following, we give a brief discussion on the possible sources of the discrepancies between theory and experiment. First, to make the computations time efficient, we used inexpensive semiempirical electronic structure models. This leads to particularly large estimates of the mode energies of the symmetric and antisymmetric NO_2 stretches in PETN. As suggested above, replacement of these simple models by DFT should improve accuracy in the normal-mode determination and accordingly in the calculations of anharmonic couplings, albeit at considerable increase in computational expense. Another issue is the use of the third- and fourth-order perturbation theory expressions for linewidth calculations [Eqs. (3)–(5)] adopted in this study. The higher-order terms which we omitted here can, in principle, provide significant contributions and might become quite important if strongly driven energy up-pumping processes such as shock initiation in PETN are considered. Finally, the energy surface calculations have been performed in the $\mathbf{\Gamma}$ point of the Brillouin zone. As such, we have not accounted accurately for the mode eigenenergies and anharmonicity dispersion relations; instead, we have made phenomenological assignments of widths to the vibrational states. While this improves the calculations, the acoustic phonons are still neglected. One way to improve this issue would be to consider "supercells" comprised of multiples of the crystallographic unit cells considered here. While this would be feasible for the semiempirical methods used in the present work, such an approach would be near the edge of practical feasibility using more accurate model chemistries.

IV. CONCLUSIONS

We have developed a computational approach that yields anharmonic vibrational couplings in molecular crystalline materials. We have implemented it for semiempirical electronic structure methods with periodic boundary conditions. The technique was applied to naphthalene and PETN crystals, allowing us to evaluate the vibrational anharmonic couplings. Experimental observables such as IR and Raman linewidths and averaged anharmonic constants have been calculated. These, and temperature-dependent Raman spectra, were compared to experiment, and reasonable agreement was obtained. From these comparisons, we conclude that the method presented here is suitable for qualitative analysis of the cubic and quartic anharmonicities in periodic molecular structures and can be applied productively to the study of certain processes of interest, for example, up- and down-conversions in shock loaded energetic materials. However, we stress that the proposed approach is general and can be used to study other kinds of systems such as molecular aggregates, (bio)polymers, and nanomaterials, for instance, carbon nanotubes.[31] Finally, the method can be extended to investigate the anharmonic vibrational couplings in photoexcited electronic states.

Further improvements in accuracy can be obtained by replacement of the approximate electronic structure theory used here by first-principles electronic structure calculations such as DFT, and modifications in either $\mathbf{k}$ space or real space that lead to better inclusion of the phonon and/or vibron-dispersion relations that are currently treated phenomenologically. While the validation obtained here by comparisons between theoretical and experimental IR and Raman linewidths is limited due to a large amount of averaging in the experiments to which we compared, a far greater degree of mode subjectivity should be attainable using nonlinear techniques such as IR and Raman multidimensional spectroscopies.[1,32–34] Confrontation with those kinds of de-

tailed data would provide a significantly greater validation challenge to the present theoretical approach.

ACKNOWLEDGMENTS

This work was supported by U.S. Department of Energy and Los Alamos Direct Research and Development Exploratory Research (LDRD-ER) programs. A.P. acknowledges support by the Center for Nonlinear Studies (CNLS).

APPENDIX: APPROXIMATE EXPRESSIONS FOR LINE-SHAPE FUNCTIONS

It is often convenient to calculate physical quantities for a periodic crystalline structure using a **k**-space representation. In **k** space, the dispersion of the energy as a function of **k** is due to interunit-cell interactions. Since our ability to perform the normal-mode analysis and anharmonic coupling evaluations is limited to the coordinate space representation of a single unit cell interacting with its periodic replicas, it is convenient to use an approximate coordinate space representation for the line-shape functions that effectively accounts for the periodic structure of the crystal. The energy dispersion in this case is phenomenologically accounted for through the functional form adopted for the vibrational densities of states. Below, we outline, highlighting the approximations, our derivation of Eqs. (3)–(8) used for the line-shape simulations.

We start with a generic vibrational potential-energy anharmonic expansion for a molecular crystal containing L unit cells, each having M atoms which form molecules

$$V_{anh}(\xi) = \sum_{\alpha,\beta,\gamma=0}^{L} \sum_{i,j,k=1}^{M} B^{(3)\alpha\beta\gamma}_{i\,j\,k} \xi_i^\alpha \xi_j^\beta \xi_k^\gamma + \sum_{\alpha,\beta,\gamma,\delta=0}^{L} \sum_{i,j,k,l=1}^{M} B^{(4)\alpha\beta\gamma\delta}_{i\,j\,k\,l} \xi_i^\alpha \xi_j^\beta \xi_k^\gamma \xi_l^\delta, \quad \text{(A1)}$$

where ξ_i^α is the ith normal-mode displacement calculated for a unit cell α, and $B^{(3)\alpha\beta\gamma}_{ijk}$ and $B^{(4)\alpha\beta\gamma\delta}_{ijkl}$ are related anharmonic constants. Using the perturbation expansion for the Raman and IR line shape, the following third-order coordinate space expression associated with the energy down-conversion process can be obtained in a straightforward way[13,14,24–26]:

$$\Gamma^d(\omega_n) = 18L\hbar^{-1} \sum_{\beta,\gamma=0}^{L} \sum_{jk=1}^{M} |B^{(3)0\beta\gamma}_{n\,j\,k}|^2 (\bar{n}_j + \bar{n}_k + 1) \times \delta(\omega_n - \omega_j^\beta - \omega_k^\gamma), \quad \text{(A2)}$$

where we have also accounted for the fact that the interactions depend on the differences of the unit-cell coordinates β and γ. Here and below, $\bar{n}_k = [\exp(\hbar\omega_k/k_BT) + 1]$ is the vibrational level occupation number, where k_B is the Boltzmann constant and T is the temperature. Next, we introduce the vibrational density of states (DOS)

$$\rho_j(\omega) = \sum_{\alpha=0}^{L} \delta(\omega - \omega_j - \Delta\omega_j^\alpha), \quad \text{(A3)}$$

where $\omega_j \equiv \omega_j^{\alpha=0}$ and $\Delta\omega_j^\alpha = \omega_j^\alpha - \omega_j$, and transform Eq. (A2) into the quasicontinuous energy representation

$$\Gamma^d(\omega_n) = 18L\hbar^{-1} \sum_{jk=1}^{M} \int d\omega' \int d\omega'' |B^{(3)}(\omega_n, \omega', \omega'')|^2 \times [\bar{n}(\omega') + \bar{n}(\omega'') + 1] \rho_j(\omega') \rho_k(\omega'') \delta(\omega_n - \omega' - \omega''). \quad \text{(A4)}$$

Integration over $d\omega''$ and change of variable $\omega' = \omega_j + \omega$ simplify this expression to the form

$$\Gamma^d(\omega_n) = 18L\hbar^{-1} \sum_{jk=1}^{M} \int d\omega \times |B^{(3)}(\omega_n, \omega_j + \omega, \omega_n - \omega_j - \omega)|^2 \times [\bar{n}(\omega_j + \omega) + \bar{n}(\omega_n - \omega_j - \omega) + 1] \times \rho_j(\omega_j + \omega) \rho_k(\omega_n - \omega_j - \omega). \quad \text{(A5)}$$

The first approximation, applied at this point, is to expand the population factors $\bar{n}(\omega_j + \omega)$ and $\bar{n}(\omega_n - \omega_j - \omega)$ in power series of ω and retain only the zero-order terms

$$\Gamma^d(\omega_n) = 18L\hbar^{-1} \sum_{jk=1}^{M} \int d\omega \times [|B^{(3)}(\omega_n, \omega_j + \omega, \omega_n - \omega_j - \omega)|^2 \times \rho_j(\omega_j + \omega) \rho_k(\omega_n - \omega_j - \omega)] \times [\bar{n}(\omega_j) + \bar{n}(\omega_n - \omega_j) + 1]. \quad \text{(A6)}$$

Our next, central approximation is to introduce effective, that is, averaged over the energy spectrum weighted by the DOS, anharmonicity couplings. These quantities are available from our simulations, since the averaging is similar to accounting for the intercell interaction associated with the periodic boundary condition

$$B^{(3)}_{ijk} \equiv L^{-3} \int d\omega |B^{(3)}(\omega_n, \omega_j + \omega, \omega_n - \omega_j - \omega)|^2 \times \rho_j(\omega_j + \omega) \rho_k(\omega_n - \omega_j - \omega), \quad \text{(A7)}$$

where the prefactor L^{-3} originates from the normalization per integrals over DOS [i.e., $L = \int d\omega \rho_j(\omega)$]. As a result, the line-shape component in Eq. (A6) can now be represented in the following form:

$$\Gamma^d(\omega_n) = 18\hbar^{-1} \sum_{jk=1}^{M} |B^{(3)}_{njk}|^2 [\bar{n}(\omega_j) + \bar{n}(\omega_n - \omega_j) + 1] \times L^{-2} \int d\omega \rho_j(\omega_j + \omega) \rho_k(\omega_n - \omega_j - \omega). \quad \text{(A8)}$$

At this point, we partition the summation argument in Eq. (A8) into the product of the effective anharmonic coupling $|B^{(3)}_{njk}|^2$ and thermally weighted joint vibrational density of states (TJ-DOS)

$$\rho^d_{jk}(\omega_n) \equiv (\bar{n}_j + \bar{n}_k + 1) L^{-2} \int d\omega \rho_j(\omega_j + \omega) \rho_k(\omega_n - \omega_j - \omega). \quad \text{(A9)}$$

Note that in contrast to DOS, this quantity is normalized per

unity. The TJ-DOS can be calculated if the form of the DOS [Eq. (A3)] is known. We interpolate to obtain the latter from the Lorentzian function

$$\rho_j(\omega) = \frac{1}{\pi} \frac{\epsilon_j}{(\omega - \omega_j)^2 + \epsilon_j^2}, \tag{A10}$$

whose width ϵ_j is the width of a *whole* vibron or optical-phonon band centered at the jth normal-mode energy ω_j. By evaluating the integral in Eq. (A9), which contains a convolution of the Lorentzian functions, we arrive at the final expression for the TJ-DOS given by Eq. (6). This expression together with Eq. (A8) leads to Eq. (3) used in our simulations. Equations (4) and (5) along with Eqs. (7) and (8), describing the line-shape components associated with the energy up-conversion and pure dephasing, respectively, can be derived in the same way as outlined above.

*Electronic address: apiryat@anl.gov

[1] S. Mukamel, *Principles of Nonlinear Optical Spectroscopy* (Oxford University Press, Oxford, 1995).
[2] J. R. Hill and D. D. Dlott, J. Chem. Phys. **89**, 842 (1988).
[3] H. Kim and D. D. Dlott, J. Chem. Phys. **93**, 1695 (1990).
[4] J. C. Deak, L. K. Iwaki, and D. D. Dlott, Chem. Phys. Lett. **293**, 405 (1998).
[5] J. C. Deak, L. K. Iwaki, and D. D. Dlott, J. Phys. Chem. A **102**, 8193 (1998).
[6] J. C. Deak, L. K. Iwaki, S. T. Rhea, and D. D. Dlott, J. Raman Spectrosc. **31**, 263 (2000).
[7] S. D. McGrane, J. Barber, and J. Quenneville, J. Phys. Chem. A **109**, 9919 (2005).
[8] D. D. Dlott and M. D. Fayer, J. Chem. Phys. **92**, 3798 (1990).
[9] A. Tokmakoff, M. D. Fayer, and D. D. Dlott, J. Phys. Chem. **97**, 1901 (1993).
[10] L. E. Fried and A. J. Ruggiero, J. Phys. Chem. **98**, 9786 (1994).
[11] V. K. Jindal and D. D. Dlott, J. Appl. Phys. **83**, 5203 (1998).
[12] D. D. Dlott, Annu. Rev. Phys. Chem. **37**, 157 (1986).
[13] S. Califano, V. Schettino, and N. Neto, *Lattice Dynamics of Molecular Crystals* (Springer-Verlag, New York, 1981).
[14] R. G. Dellavalle, P. F. Fracassi, R. Righini, and S. Califano, Chem. Phys. **74**, 179 (1983).
[15] R. G. DellaValle, G. F. Signorini, and P. Procacci, Phys. Rev. B **55**, 14855 (1997).
[16] W. F. Perger, S. Vutukuri, Z. A. Dreger, Y. M. Gupta, and K. Flurchick, Chem. Phys. Lett. **422**, 397 (2006).
[17] W. F. Perger, J. Zhao, J. M. Winey, and Y. M. Gupta, Chem. Phys. Lett. **428**, 394 (2006).
[18] Y. A. Gruzdkov and Y. M. Gupta, J. Phys. Chem. A **105**, 6197 (2001).
[19] M. J. S. Dewar, E. G. Zoebisch, E. F. Healy and J. J. P. Stewart, J. Am. Chem. Soc. **107**, 3902 (1985).
[20] J. J. P. Stewart, J. Comput. Chem. **10**, 209 (1989).
[21] J. J. P. Stewart, J. Comput. Chem. **10**, 221 (1989).
[22] J. J. P. Stewart, MOPAC 2002, Schrödinger Inc. and Fujitsu Limited, Portland, OR 2000.
[23] G. Schaftenaar and J. Noordik, J. Comput.-Aided Mol. Des. **14**, 123 (2000).
[24] A. A. Abrikosov, L. P. Gorkov, and I. E. Dzyaloshinski, *Methods of Quantum Field Theory in Statistical Physics* (Dover, New York, 1963).
[25] A. A. Maradudin and A. E. Fein, Phys. Rev. **128**, 2589 (1962).
[26] S. Califano and V. Schettino, Int. Rev. Phys. Chem. **7**, 19 (1988).
[27] J. Oddershede and S. Larsen, J. Phys. Chem. A **108**, 1057 (2004).
[28] J. W. Conant, H. H. Cady, R. R. Ryan, J. L. Yarnell, and J. M. Newsam, Los Alamos Scientific Laboratory Report No. LA-7756-MS, 1979.
[29] J.-L. G. D. Paz and J. Ciller, Propellants, Explos., Pyrotech. **18**, 33 (1993).
[30] J. Zhang, H. M. Xiao, and X. D. Gong, J. Phys. Org. Chem. **14**, 583 (2001).
[31] A. Gambetta, C. Manzoni, E. Menna, M. Meneghetti, G. Cerullo, G. Lanzani, S. Tretiak, A. Piryatinski, A. Saxena, R. L. Martin, and A. R. Bishop, Nat. Phys. **2**, 515 (2006).
[32] S. Mukamel, A. Piryatinski, and V. Chernyak, Acc. Chem. Res. **32**, 145 (1999).
[33] *Ultrafast Infrared and Raman Spectroscopy*, edited by M. D. Fayer (Dekker, New York, 2001).
[34] S. Mukamel and D. Abramavicius, Chem. Rev. (Washington, D.C.) **104**, 2073 (2004).